Ceramics International xxx (xxxx) xxx

Contents lists available at ScienceDirect

Ceramics International

journal homepage: www.elsevier.com/locate/ceramint

From high-volume industrial waste to new ceramic material: The case of red gypsum muds in the TiO_2 industry

Narcisa Mihaela Marian [a,*], Matteo Perotti [a], Carlo Indelicato [a], Claudia Magrini [a], Giovanna Giorgetti [a], Giancarlo Capitani [b], Cecilia Viti [a,**]

[a] Department of Physical Science, Earth and Environment DSFTA (UniSi), V. Laterina 8, I-53100, Siena, Italy
[b] Department of Earth and Environmental Sciences DISAT (UniMIB), Piazza della Scienza, 4, 20126, Milano, Italy

ARTICLE INFO

Keywords:
A Sintering
B Electron microscopy
B X-ray methods
D TiO_2

ABSTRACT

The present study aims to apply the principles of circular economy, using special inorganic waste (in particular, red gypsum muds from a TiO_2 plant in Tuscany, Italy) to produce ceramic materials for the construction and building industries. Red gypsum (RG) muds produced during more than 10 years of industrial processing were chemically and mineralogically characterized by X-ray fluorescence spectrometry (XRF), X-ray powder diffraction (XRPD), scanning electron microscopy with energy dispersive X-ray spectrometer (SEM/EDS), and thermal analyses (TA). The analyses testify that RG waste production is chemically and mineralogically constant over time, and therefore suitable to be used as a secondary raw material in industrial ceramic production. Ceramic specimens have been realized using an extremely high amount of the RG waste (up to 70%) and characterized using the same chemical-mineralogical techniques, revealing that anhydrite, pyroxene, and Fe/Ti oxides are the main crystalline phases, embedded in a glassy compact matrix. Overall results indicate that the production of ceramic materials could represent a definitive and sustainable solution for the problematic management of the large volumes of RG waste deriving from TiO_2 plants.

1. Introduction

Mineral resources are essential raw materials of everyday commodities, from common ceramics and building materials to high-tech and nanotechnological devices. Most mineral resources are not renewable, at least on the human time scale. In other words, there is a time-scale gap between the human exploitation/consumption of natural resources and the geological times required by our planet to restore what is consumed. This poses severe problems for the future availability of natural raw materials, and strategies alternative to the massive exploitation of natural resources until their exhaustion, are immediately needed [1,2].

The industrial processes that transform raw mineral resources into various industrial products typically require physical and/or chemical treatments of the raw material. In most cases, this implies chemical reactions with the consequent production of highly polluting, acid wastewater. In other words, the use of natural resources and the realization of commercial products are inevitably associated with the production of waste at any stage of the product life cycle, therefore requiring an adequate management strategy [3].

Gypsum waste is commonly produced in the construction and demolition industry, but huge amounts also arise from TiO_2 production plants [4–6]. The industrial process to extract Ti from the ore mineral ilmenite ($FeTiO_3$) [7–10] results in the formation of acid wastewater, which are successfully neutralized with $CaCO_3$ powder [11]. The neutralization reaction of acid wastewater with calcite powder represents therefore a step in environmental protection, despite inevitably resulting in another environmental issue. In fact, the neutralization reaction H_2SO_4 (aq) + $CaCO_3$ → $CaSO_4{\cdot}2H_2O$ + CO_2 produces considerable volumes of gypsum mud (7/8 tons of gypsum waste for 1 ton of TiO_2 production), characterized by a red color due to the occurrence of minor Fe-bearing phases deriving from the raw mineral ilmenite. Although red gypsum (hereafter RG) (in accordance with European Waste Catalogue

* Corresponding author.
** Corresponding author.
E-mail addresses: narcisamihaela.ma@student.unisi.it (N.M. Marian), cecilia.viti@unisi.it (C. Viti).

https://doi.org/10.1016/j.ceramint.2023.01.086
Received 13 September 2022; Received in revised form 26 December 2022; Accepted 10 January 2023
Available online 11 January 2023

code 061101) mud is a non-hazardous waste, it is classified as a special industrial waste that needs to be managed [6,12,13].

Managing large volumes of RG waste is an environmental, social, and political problem that needs to be addressed soon. The most adopted solution so far has been the environmental restoration of abandoned quarries, mines, and landfills where RG is used as inert material to restore the original morphology of the area. Unfortunately, social communities do not always appreciate environmental restoration due to possible geochemical and hydrogeological concerns, despite scientific data supporting this solution's safety [14–16].

A promising alternative, in agreement with environmental protection issues, sustainable exploitation of natural resources, and circular economy, is to reuse RG wastes as secondary raw materials [17]. Previous studies explored the possible reuse of gypsum wastes in the cement and building materials industry [18–21]. It was demonstrated that using RG instead of natural gypsum in Portland cement manufacture maintains the physico-mechanical properties and the leaching behavior of the final product [18]. Zhang et al. [20] also studied the use of RG to produce foamed Portland cement with good compressive strength and thermal insulation properties. Cai et al. [21] demonstrated the possible use of up to 20% RG as raw material to partially replace fly ash, generally composed of mullite and quartz, for the manufacturing of autoclaved aerated concrete, obtaining good physical and mechanical properties. Moreover, RG by-products have been also tested as raw materials in manufacturing gypsum blocks for the building and construction industry [19]. Fauziah [22] investigated the possibility of using RG in combination with sewage sludge and soil in different proportions in the agricultural environment as an amendment and a source of Ca for plants.

The present study fits into this context. RG wastes deriving from a TiO_2 industrial plant (Tuscany, Italy) have been investigated to confirm their chemical and mineralogical homogeneity over more than 10 years of industrial production and to verify the possible occurrence of toxic elements above normative limits. Subsequently, the investigated RG wastes have been used as a secondary raw material to produce an innovative thermoformed ceramic material, following the procedures described in patent n. 0001369219, released by the Italian Patent and Trademark Office on 11/01/2010 (owner GRINN Solutions s.r.l.). The resulting ceramics, realized using a high quantity of gypsum waste from 60 to 70% and characterized by excellent aesthetic, mechanical, and physical properties, may represent a competitive material in the ceramic trade, thus representing a promising example of the circular economy.

2. Samples and analytical method

Four representative samples of RG wastes (RG1-RG2-RG3-RG4), produced in an industrial plant located in Tuscany (Italy) for more than 10 years of production (Table 1S) were analyzed. Samples RG1 (the oldest: 2010) and RG4 (the youngest: July 2021) have been used to produce 2 ceramic tiles (hereafter, samples CRG1 and CRG4, respectively; Fig. 1S), following the procedures described in the patent and summarized below (paragraph 4 RG WASTE PROCESSING). CRG1 has a size of 4 cm length x 2 cm width x 0.7 cm height, while CRG4 one is round shape with 6 cm in diameter and 1 cm high. Both RG untreated samples and CRG resulting ceramic products have been analyzed with different mineralogical techniques.

X-ray powder diffraction (XRPD) analyses were carried out with a Bragg-Brentano Philips X'Pert PRO PW3050/60 diffractometer (CuKα radiation, operating conditions of 40 kV and 30 mA), equipped with PW3071 X'Celerator detector, 3–80° 2θ range, allowing the accurate determination of the bulk mineralogical composition of both RG samples and CRG samples. Before the analyses, small quantities (a few mg) of RG and CRG samples were finely grounded in an agate mortar.

Energy dispersive X-ray fluorescence spectrometry (EDXRF) for chemical bulk analysis was performed on samples prepared by mixing approximately 15 g of powdered material with 5 g of boric acid and a few drops of polyvinyl alcohol. Powders were then pressed under a laboratory press (20 t/cm^2) compacted into pellets of 40 mm of diameter and finally analyzed with the PANalytical Epsilon 3XL instrument. The Omnian-standardless method was used for quantitative analyses. Volatile components (H_2O plus CO_2) were determined through the weight loss on ignition (LOI). The Fe^{3+}/Fe^{2+} ratio was determined through $KMnO_4$ redox titration.

Thermal analyses (TA) were carried out on a few mg (17–37) starting untreated RG wastes to check their thermal behavior during heating. TA (thermogravimetry, TG, differential thermogravimetry DTG, and differential thermal analysis, DTA) were obtained by a simultaneous DSC/TGA Thermal analyzer Q600 TA instruments, applying a heating rate of 10 °C/min, from room temperature to 1000 °C, in 20 ml/min airflow.

Scanning Electron Microscope (SEM) analyses were carried out with a TESCAN VEGA 3 working at 20 kV of accelerating voltage, 15 μA of emission current, and 0.1 nA of beam current. The microscope is equipped with an energy-dispersive X-ray spectrometer (EDS) Bruker Quantax 200EDX for chemical microanalysis with P/B - ZAF correction method. Natural minerals were used as standards for EDS calibration. RG powders have been dispersed on adhesive carbon tape stuck above SEM aluminum stubs, whereas CRG tiles were cut to realize polished petrographic sections, 33 mm length x 20 mm width x 30 μm thickness; both powders and polished sections were carbon-coated before SEM observations. SEM images of CRG samples were analyzed with the particle image analysis software (FIJI/ImageJ [23]), focusing on 2D porosity determination. Five representative back-scattered electrons (BSE) images were collected for each sample at low magnification (150x), and then smoothed, filtered, and thresholded. Binarization aims to obtain a two colors image to elaborate successive segmentation, to determine areas occupied by the ceramic material and areas occupied by 2D pores. Once binarized and segmented, images were processed with the particle analysis tool of Image/J. A minimum threshold of 1 μm^2 was chosen to analyze particles. The obtained porosity value is the average ratio (%) between the area occupied by pores and the total area of each image.

The research methodology showing the main analyses made on RG and CRG samples, is summarized in the flowchart in Fig. 1.

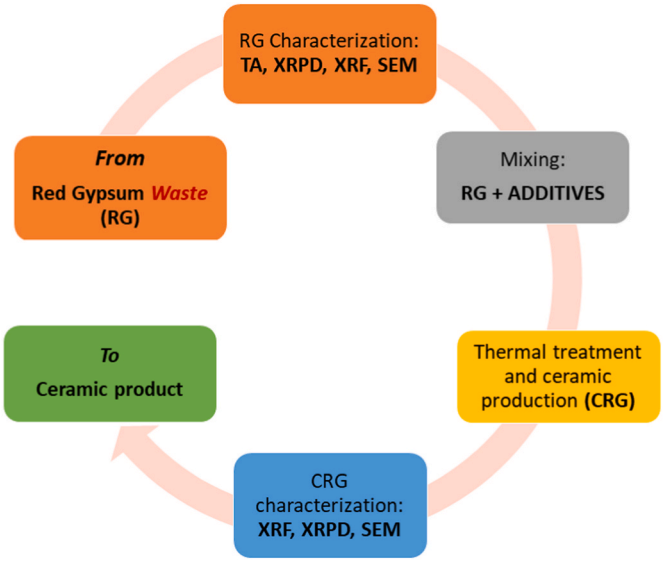

Fig. 1. Flowchart showing the frame of the performed investigation.

Table 1
EDXRF bulk data (wt% oxides) for the four RG samples and two ceramic samples CRG1 and CRG4.

wt%	RG1	RG2	RG3	RG4	CRG1	CRG4
Na_2O	0.74	0.46	0.36	0.51	1.24	1.16
MgO	2.46	1.06	2.17	3.91	1.22	0.93
Al_2O_3	1.25	1.18	1.24	0.80	4.66	4.61
SiO_2	2.31	1.94	2.16	1.46	19.65	19.78
P_2O_5	0.03	0.03	0.03	0.03	*n.d.*	*n.d.*
SO_3	38.45	38.53	37.25	38.76	35.49	35.80
Cl	0.67	0.03	0.10	0.34	*n.d.*	*n.d.*
K_2O	0.12	0.09	0.06	0.05	0.40	0.33
CaO	29.30	30.23	29.11	27.48	28.35	25.49
TiO_2	1.29	1.14	1.43	1.38	1.21	1.13
V_2O_5	0.18	0.13	0.16	0.13	0.14	0.11
Cr_2O_3	0.06	0.05	0.05	0.04	0.13	0.05
MnO	0.08	0.11	0.11	0.15	0.08	0.11
Fe_2O_3	3.97	3.52	4.57	3.90	3.97	3.58
CuO	*n.d.*	*n.d.*	*n.d.*	*n.d.*	*tr*	*tr*
ZnO	*n.d.*	*n.d.*	*n.d.*	*n.d.*	0.06	0.06
SrO	0.02	0.02	0.03	0.02	*tr*	*tr*
ZrO_2	*n.d.*	*n.d.*	*n.d.*	*n.d.*	0.18	0.19
SnO_2	0.02	0.02	0.02	0.02	0.46	0.41
BaO	0.00	0.01	0.01	0.01	0.49	0.49
NiO	0.01	n.d.	n.d.	n.d.	*n.d.*	*tr*
PbO	*n.d.*	*n.d.*	*n.d.*	*n.d.*	0.17	0.13
LOI	19.05	21.46	21.15	21.01	1.87	5.42
Total	100.00	100.00	100.00	100.00	99.79	99.79

Note: LOI = loss on ignition, n.d. = not detected, tr = trace.

3. The red gypsum waste: chemical, mineralogical and microstructural characterization

RG samples are macroscopically comparable, with homogeneous color and grain size. Table 1 reports the XRF bulk composition of the four samples revealing that they are constantly formed by SO_3 (37–38 wt %) and CaO (27–30 wt%) with minor Fe_2O_3, TiO_2, SiO_2, Al_2O_3, and MgO. We also remark on the occurrence of trace elements Cr and V (here expressed as wt% oxides Cr_2O_3 and V_2O_5), reasonably resulting from the original raw mineral ilmenite and important for possible environmental concerns. The volatile content, ranging from ~19 to ~21 wt%, was estimated through thermal analyses to better discriminate the loss between hygroscopic water (humidity) and structural water of gypsum which led to mineralogical transformation first to hemihydrate and then to anhydrite.

Thermal analyses allowed us to investigate the transformation of gypsum into anhydride, with a theoretical overall weight loss of approximately 20–21%. Gypsum dehydration occurs in two separate steps: i) in the first step, gypsum transforms to hemihydrate, close to 128 °C, with a weight loss of 13–14 wt%; ii) in the second step, hemihydrate transforms to anhydrite, close to 158/160 °C, with a weight loss of 6–7 wt% [24–27].

TG, DTG and DTA results for our gypsum samples are reported in Fig. 2 (green, red and blue lines, respectively), whereas main TG losses and temperatures of main DTG and DTA signals are summarized in Table 2. TG data and LOI indicate a highly variable weight loss from room temperature to 100 °C (from 1.60 wt% up to 17.11 wt%), associated with endothermic signals in the range 55–84 °C. The observed differences in weight loss below 100 °C are probably due to samples conservation conditions and, consequently, to variable contents in

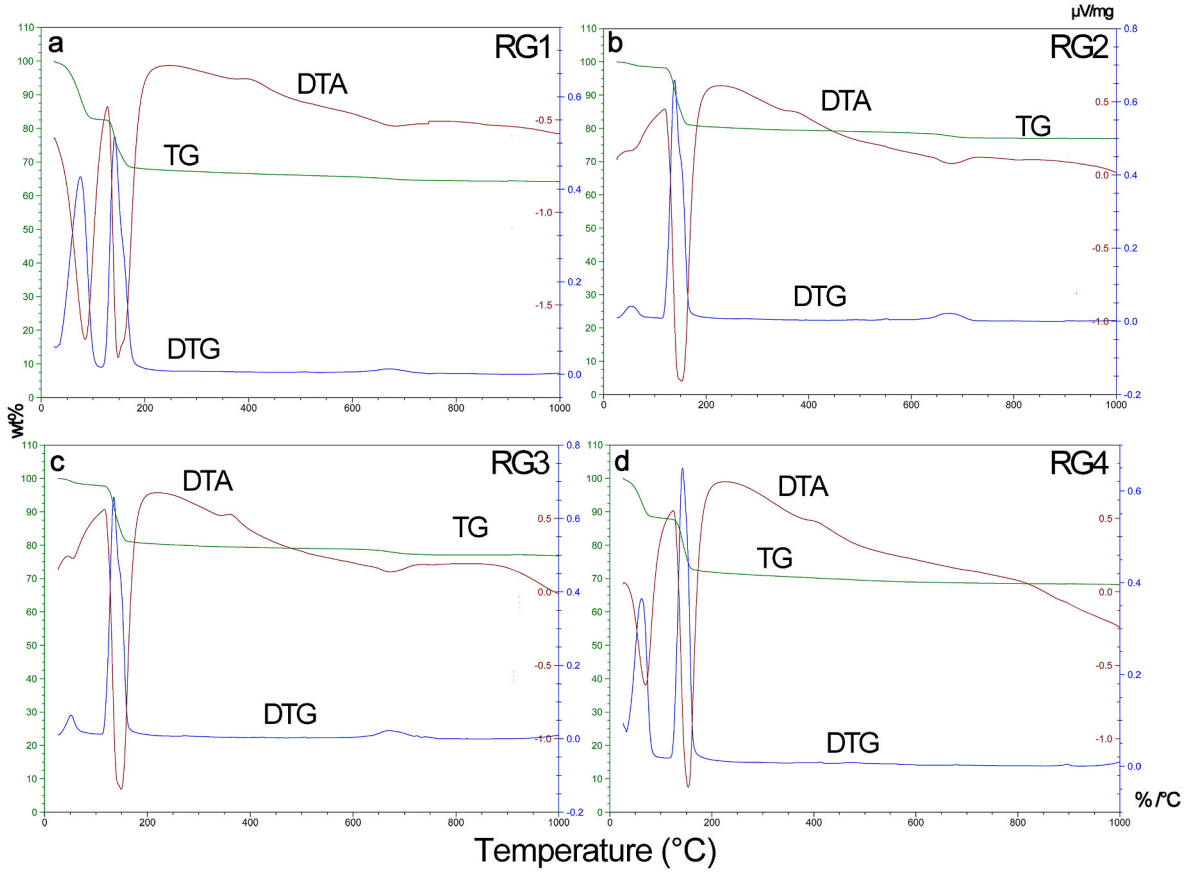

Fig. 2. Thermal analysis of the four RG samples, in air, heating rate of 10 °C/min, in the range 0–1000 °C; DTA exothermal signals are upwards. Green curve: thermogravimetric analysis (TG); blue curve: differential thermogravimetry (DTG); red curve: differential thermal analysis (DTA). (For interpretation of the references to color in this figure legend, the reader is referred to the Web version of this article.)

Table 2
Main TG, DTG, and DTA data for the samples RG1, RG2, RG3, and RG4. The abbreviations w (weak), s (strong), and vs (very strong, main peak) are arbitrary and are based on a qualitative observation of the peak's height.

TG data							
RG1		RG2		RG3		RG4	
T range (°C)	TG loss %	T range (°C)	TG loss %	T range (°C)	TG loss %	T range (°C)	TG loss %
RT-100	17.11	RT-100	1.60	RT-100	2.06	RT-100	11.86
100–180	15.00	100–180	17.60	100–180	17.15	100–180	15.87
180–600	2.71	180–600	2.16	180–600	2.00	180–600	3.30
600–1000	1.34	600–1000	1.70	600–1000	2.00	600–1000	0.84
total weight loss 100 - 1000	19.05	total weight loss 100 - 1000	21.46	total weight loss 100 - 1000	21.15	total weight loss 100 - 1000	20.01
DTG peak temperature in DTG curves (°C)							
RG1		**RG2**		**RG3**		**RG4**	
75 s		52 w		52 w		62 s	
140 vs		138 vs		134 vs		142 vs	
155 sh		151 sh		147 sh			
672 w		675 w		672 w			
DTA peak temperature in DTA curves (°C)							
RG1		**RG2**		**RG3**		**RG4**	
84 s endo		58 w endo		55 w endo		70 s endo	
148 vs endo		145 vs endo		141 vs endo			
158 sh endo		152 sh endo		149 sh endo		153 vs endo	
399 w exo		376 w exo		360 w exo		403 w exo	
683 w endo		675 w endo		673 endo			

Note: RT = room temperature, w = weak, s = strong, vs = very strong (main peak), sh = shoulder endo = endothermic, exo = exothermic.

atmospheric adsorbed water. Main weight loss occurs in the range of 100–180 °C (from 15.00 wt% to 17.60 wt%), due to the progressive dehydration from gypsum to hemihydrate and lastly into anhydrite. The width and asymmetric shape of DTG and DTA peaks in the 100–180 °C range (especially evident for samples RG1-RG2 and RG3; Fig. 2S) reflect the two-step dehydration of gypsum (e.g., the wide and asymmetric endothermic signal in the 141–158 °C range). At higher temperatures (range 180–600 °C), weight loss is very low (2.00–3.30 wt%), whereas is remarkable the occurrence of a weak exothermic peak (360–403 °C) that has been interpreted as due to the transformation of soluble anhydrite (γ) to insoluble anhydrite (β) [28–31]. Weight loss in the 600–1000 °C range is negligible (0.84–2.00 wt%), whereas is visible a weak endothermic signal at 673–683 °C, possibly caused by dehydration of minor Fe-bearing phases [24].

Total weight losses for the four gypsum wastes in the range 100–1000 °C range from 19.05 to 21.46 wt%, in agreement with the expected loss for pure gypsum samples.

XRPD patterns confirm that RG wastes are almost exclusively formed by gypsum, with rare occurrence of quartz (Fig. 3). Fig. 3 reports gypsum main reflections, with *hkl* lattice planes (brackets) and corresponding interplanar distance (d). Red arrows indicate some minor peaks belonging to gypsum, particularly evident in samples RG1, RG2, and RG3, with interplanar distances of 2.87 Å, 2.79 Å, and 2.68 Å, corresponding respectively to 200, 112, 220 *hkl* lattice planes. The grey arrows identify the main peak of quartz corresponding to the 3.35 Å-spaced (101) lattice planes [32,33]. XRD data, therefore, confirm that wastes deriving from more than 10 years of TiO_2 production are almost exclusively formed by gypsum.

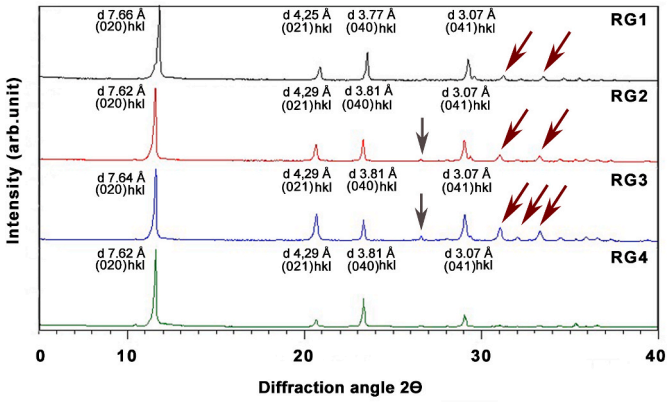

Fig. 3. XRPD patterns of untreated RG wastes, with main (*hkl*) reflections and corresponding d-spacings (Å); red arrows indicate some minor peaks always belonging to gypsum, whereas grey arrow identifies the main peak of quartz corresponding to 3.35 Å-spaced (101) lattice planes. (For interpretation of the references to color in this figure legend, the reader is referred to the Web version of this article.)

SEM observations reveal minor microstructural differences between the RG samples, as observed in Fig. 4, where the four samples are compared at the same magnification (300X, Fig. 4). Fig. 4A and C shows euhedral crystals (highlighted with the line drawing) with the typical gypsum twinning ("fishtail" or "swallowtail" twinned crystals), whereas Fig. 3B and D highlight not-twinned euhedral crystals with a tabular prismatic habit (line drawing). The crystal size of the four gypsum samples is comparable, ranging from ~20 μm to ~200 μm.

The images E and F in Fig. 4 are representative of two common minor phases that were not detected by XRPD due to their extremely low amount, in particular, Ti- and Fe-oxides. The Ti- and Fe-oxide grains, bright in BSE images, have grain sizes below 20–30 μm and exhibit subhedral habits, suggesting that they arise from the primary raw material rather than from the acid waste de-activation process leading to gypsum formation. Careful SEM/EDS analyses also allowed for the detection of rare Fe and Ti oxide grains slightly enriched in Cr and V, coherently with XRF results. The above heavy elements do not occur in the gypsum crystal structure, as confirmed by EDS analyses.

4. RG waste processing

Ceramic tests CRG1 and CRG4 have been realized using approximately 70% of unaltered red gypsum (no grinding process was done), mixed with variable additives, predominantly: i) amorphous silica; ii) Na-silicates, in variable proportions. The samples were pressed and formed under wet conditions (about 20–30% of humidity), and then treated in a furnace at slightly different conditions, i.e., at 920 °C and 1000 °C, for 60 and 30 min, respectively. Both samples' heating rate was set up at 100 °C/h. Further technical details cannot be disclosed due to the patent trade secret.

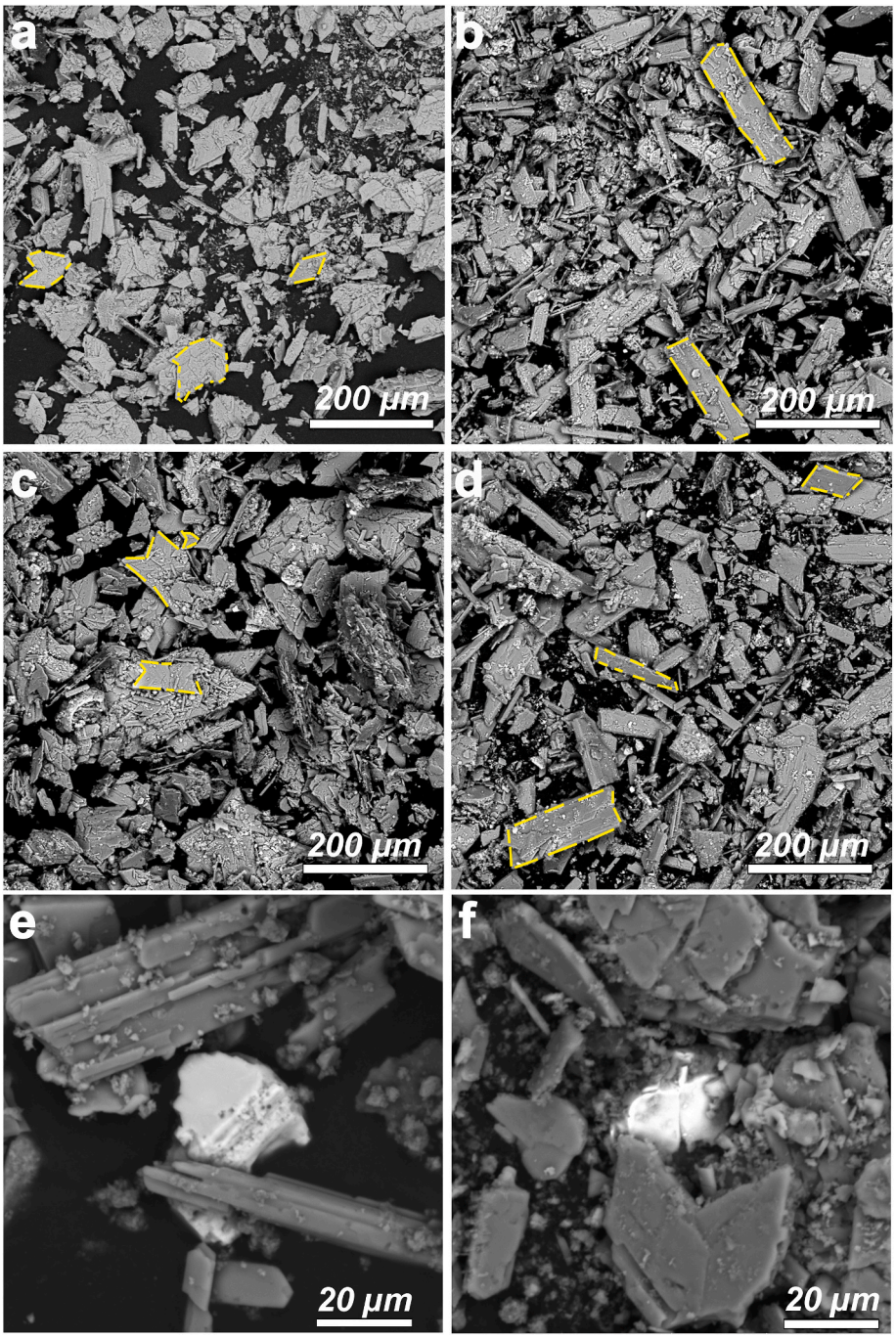

Fig. 4. BSE SEM images of the RG samples. a) Gypsum in RG1 sample, with common twinned crystals; b) Gypsum in RG2 sample with predominant not-twinned euhedral tabular crystals; c) Gypsum in RG3 sample, with common twinning; d) Gypsum in RG4 samples, with predominant tabular habit and rare twinned crystals; e and f) Representative images of Fe and Ti – oxides respectively occurring in gypsum samples.

5. The ceramic products: chemical, mineralogical and microstructural properties

The two analyzed ceramic products appear different at a macroscopic observation (Fig. 1S A and B for CRG1 and CRG4, respectively), particularly for the different color (variable with the used additives). In Fig. 3S it is possible to observe analogous ceramic products to those studied here, realized with the above patent and with red gypsum. The two samples have been in part powdered (for XRF and XRD analyses) and cut to realize thin polished petrographic sections (for optical microscopy and SEM/EDS observations).

Table 1 reports, in the last two columns, XRF bulk data for CRG samples. The ceramic products are mainly composed of SO_3 (~35–36 wt %), CaO (~25–28 wt%), and SiO_2 (~20 wt%) with minor Al_2O_3, Fe_2O_3 Na_2O, TiO_2 and MgO.

Minor differences between the two ceramic products are reasonably due to slight variation in the starting ceramic batch, particularly for what concerns the CaO content and volatile content values. It is remarkable that undesired heavy elements, such as Cr and V, occur in limited amounts.

Fig. 5 reports XRPD patterns of the two samples, showing a good reproducibility of the ceramic production process (black and red lines for CRG1 and CRG4, respectively). The main crystalline phase is anhydrite (blu line), deriving from gypsum dehydration, with minor augite-

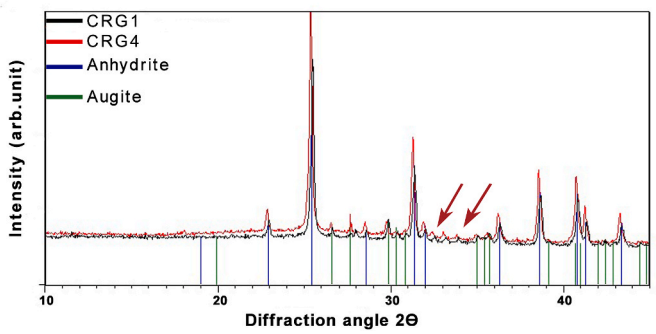

Fig. 5. XRPD patterns of the CRG1 (red line) and CRG4 (black line); blue lines correspond to anhydrite peaks, whereas the green ones correspond to the silicatic phase, pyroxene. Minor hematite and cassiterite are pointed out by the arrows. (For interpretation of the references to color in this figure legend, the reader is referred to the Web version of this article.)

like pyroxene (green line), which represents the new high-T crystalline phase formed from the silicatic flux. Arrows correspond to the main peaks of hematite (Fe_2O_3), probably resulting from the raw starting material, and cassiterite (SnO_2), which conversely has been added to the ceramic batch, probably to improve the aesthetic properties of the ceramic product.

SEM/BSE observations on the two polished petrographic sections reveal broadly similar microstructures, even if significant differences can be observed for what concerns pyroxene crystal size, pore size and distribution (e.g., Fig. 6).

The average apparent porosity of the two investigated samples obtained from image analysis is quite different, reflecting the ceramic oven's slightly different temperatures and time conditions. CRG1 has an average porosity value of 22%, while CRG4 is less porous (12%), as evident in Fig. 6A and D and in Fig. 4S A and B where are reported the two pore size distribution histograms. Pore size ranges from 8 to 450 μm for CRG1 and from 8 to 330 μm for CRG4. In both samples, pore shape is variable, from rounded to irregular (e.g., arrows in Fig. 6A and D), whereas the aspect ratio (i.e., the ellipticity of pores) shows greater variability in sample CRG4. Full image analysis data are available in Table 2S and Fig. 4S in the supplementary materials.

The ceramic products comprise a glassy and compact matrix, hosting the different crystalline phases (Fig. 6B and C and 6E-F for CRG1 and CRG4, respectively). The observed crystalline phases are (from the more to the less abundant): 1) anhydrite (pale grey) which is the most abundant crystalline phase in both samples (e.g., anh in Fig. 6C and F). Anhydrite is characterized by an evident parallel fissure system ("shrunk structure"), consequent to the significant volume reduction during the gypsum-to-anhydrite phase transition; 2) augitic pyroxene (pale grey), in elongated and skeletal crystals, up to 10 × 2 μm and 50 × 10 μm in CRG1 and CRG4, respectively (px and yellow line drawing in Fig. 6C and F); 3) cassiterite (SnO_2), characterized by the highest BSE coefficient, in rounded sub-euhedral crystals, 5–10 μm in size (e.g., cst in Fig. 6C and F); 4) Ti-rich iron oxides, typically occurring in tiny (up to 5 × 1 μm) acicular crystals (e.g., Ox Fe and Ti in Fig. 6F); 5) Fe oxides, in euhedral crystals with high BSE coefficient, 5–10 μm in size (Ox-Fe in Fig. 6C and F).

The grain size of anhydrite crystals are equivalent in the two samples and are substantially inherited by the size of starting gypsum crystals. Conversely, the size of augitic crystals, and pore distribution, clearly indicate a more evolved annealing in CRG4 with respect to CRG1. This is probably due to slightly different processing and heating conditions, in particular, the maximum temperature reached, 1000 °C, and the stationing heating time, 30 min, for CRG4 [34–37]. As regards minor phases, such as cassiterite, Fe and Ti-rich Fe oxides, microstructural features do not allow to understand if crystals are the same as the original starting batch or if they have experienced high-T recrystallization in the ceramic kiln.

Table 3 reports EDS representative chemical analyses for glass matrix, anhydrite, pyroxene, Fe oxides and cassiterite (see also Table 3S reporting the maximum, minimum and mean value for each phase of ceramic materials, expressed in wt% oxides). Some point analyses are reported in Figs. 5S and 6S of supplementary analyses.

The glassy matrix has a similar composition in both samples and is mostly composed of SiO_2, Al_2O_3, Na_2O and CaO, together with minor FeO and MgO, deriving from the additives used in the starting ceramic batch. The measured TiO_2, SnO_2 and SO_3 contents could be due to the large volume analysis, possibly resulting from contamination (i.e., the occurrence of tiny grains of Ti-rich oxide, cassiterite and gypsum in the analyzed matrix volume). Conversely, EDS data suggest that V_2O_5 is preferentially partitioned in the glassy matrix, showing the highest detected values.

Ca-pyroxenes reveal composition intermediate between augite and diopside, with representative atoms per formula units (a.p.f.u.) of Si

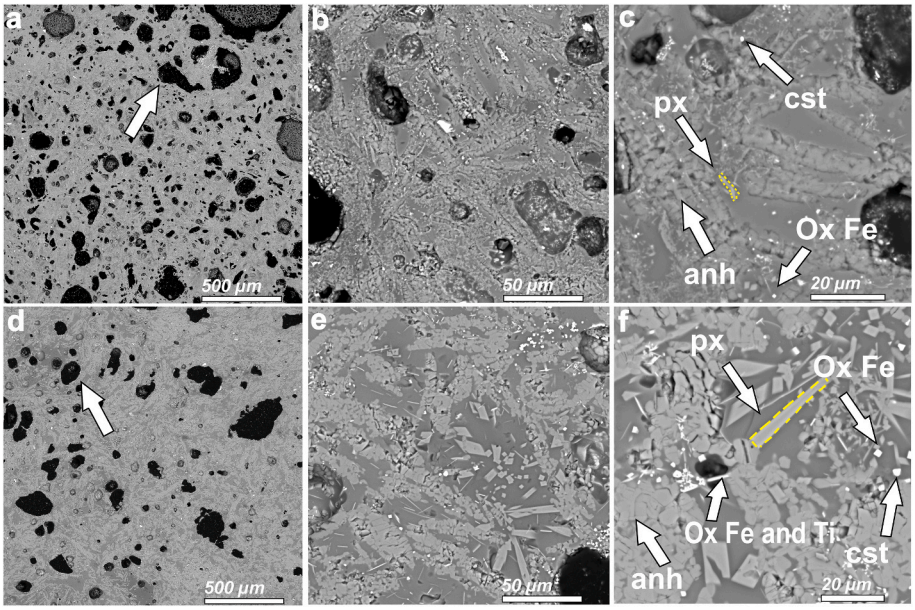

Fig. 6. SEM BSE images of the two CRG samples (upper row: sample CRG1; lower row: sample CRG4; images in column have been collected at the same magnification). Images A and D have highlighted the relevant differences in pore size and pore distribution in the two ceramic products. Images B and E allow remarking the significantly different crystal size (especially for pyroxene), which is larger in CRG4. Images C and F show the main crystalline phases detected by SEM/EDS. Mineral labels are based on the official abbreviation and are pointed out by arrows and by line drawing, in the pyroxene case.

Table 3
EDS average compositions of glass, anhydrite, pyroxene, Fe and Ti-rich Fe oxides, and cassiterite for samples CRG1 and CRG4.

Wt%	Glass		Anhydrite		Pyroxene		Ox Fe and Ti		Cassiterite	
	CRG1	CRG4	CRG1	CRG4	CRG1	CRG4	CRG1	CRG4	CRG1	CRG4
SiO_2	57.90	57.41	1.73	1.85	52.17	47.77	7.99	12.17	9.38	4.90
Al_2O_3	11.88	13.42	0.44	0.36	8.39	7.53	2.66	3.38	2.69	1.14
MgO	4.63	2.98	0.12	0.07	9.57	8.96	1.91	4.20	0.63	0.20
FeO (tot)	4.60	4.24	0.24	0.14	6.58	10.00	70.67	55.79	0.79	0.29
Na_2O	5.66	6.16	0.43	0.12	3.89	2.94	1.89	1.61	2.11	0.72
K_2O	1.19	1.04	0.04	0.02	0.48	0.36	0.16	0.14	0.35	0.27
CaO	8.88	9.29	34.16	35.57	16.70	17.33	2.42	3.54	2.48	0.76
TiO_2	1.96	2.10	0.18	0.10	2.01	4.76	8.46	15.21	0.34	0.08
Cr_2O_3	0.01	0.01	0.00	0.01	0.04	0.03	0.29	0.23	0.01	0.01
MnO	0.09	0.25	0.08	0.04	0.17	0.33	0.42	0.58	0.00	0.02
SO_3	2.38	2.11	62.55	61.69	–	–	2.60	2.40	3.60	0.57
SnO_2	0.49	0.59	0.04	0.02	–	–	0.18	0.62	77.61	91.02
V_2O_3	0.36	0.39	0.00	0.00	–	–	0.33	0.12	0.01	0.01

1.98, $^{[IV]}$Al 0.02, $^{[VI]}$Al 0.09, Ti 0.02, Fe^{2+} 0.09, Mg 1.01, Ca 0.68, Na 0.10, K 0.01. However, also Ca-pyroxenes enriched in Na have been detected by EDS spectrometer, with a representative composition of (a. p.f.u.) of Si 1.90, $^{[VI]}$Al 0.10, $^{[VI]}$ Al0.30, Ti 0.06, Fe^{2+} 0.22, Mn 0.01, Mg 0.46, Ca 0.65, Na 0.28, K 0.03. The latter belongs to Ca–Na pyroxenes according to the classification of Morimoto [38].

EDS data for micrometric crystals, such as those of Fe oxides, Ti-rich Fe oxides and cassiterite, are typically affected by contamination drawbacks. It is however remarkable that they may host up 0.23 and 0.29 wt% in Cr_2O_3, not detected in the surrounding glassy matrix.

6. Discussion

6.1. The environmental concern of RG wastes

The environmental concern of RG wastes is directly related to the growing worldwide demand for TiO_2. The uses of TiO_2 range from the most traditional ones, i.e., paintings and pigments, to many different applications, such as special and bio-ceramics, cosmetics, gas sensing and medical devices, particularly when TiO_2 is synthesized in nanosized crystals [39–43]. The primary waste of TiO_2 industrial production are acid solutions, produced during raw material ($FeTiO_3$) processing and subsequent Ti extraction [44,45]. Acid solutions pose a more significant environmental concern with respect to RG waste, due to soil acidification and groundwater pollution. Therefore, RG, i.e., secondary waste deriving from acid solution neutralization, should be considered as the "best solution" to reduce the overall environmental impact of TiO_2 industrial production. At the same time, RG production "neutralizes" another kind of waste, that also has a huge environmental and landscape impact, i.e., the $CaCO_3$ powders deriving from extraction and processing of carbonatic lithologies (as in the case of the nearby Calcare Massiccio and Carrara Marble quarries).

The main problem in RG waste management is represented by their volumes. In Italy about 500.000 tons/year are produced, similarly to the Terengganu Malaysia plant production (400.000 tons/year) [46,47]. The Huelva's Spanish plant has a RG production of ~70.000 tons/year [11,48], whereas the Taicang plant in China has the highest impact with 15.000.000 tons/year [20,49]. One of the commonly adopted solutions for RG waste management is the environmental restoration of dismissed quarries and landfills [50,51]. As regards the studied case, from 2004 Tuscan RG wastes have been disposed in a dismissed quarry (Poggio Speranzona, nearby the TiO_2 industrial plant) after an agreement among the industrial counterpart, the Tuscany Region Council and the local municipalities where the quarry is located [52]. RG disposal was monitored by periodic geochemical analyses of soil, groundwater and aquifer, done by ARPAT (Regional Agency for Environmental Protection of Tuscany; reports available at http://www.arpat.toscana.it/), as well as by the scientific community ([14]). The comparison of chemical results obtained before and during RG disposal and at the end of site restoration, demonstrated that soil, groundwater and aquifer chemistry was constant, without significant trends of increasing or decreasing of the major ions and trace elements concentrations, thus indicates that RG was substantially inert, and they did not release undesired elements in the environment above normative limits [14,53].

Nevertheless, the social community did not appreciate this kind of solution for future disposal, raising doubts about Cr and V concentrations in water eluates and possible water sulphation. Currently, no other environmental restoration project has been approved. This implies that an alternative solution for RG waste disposal must be rapidly found. The study fits this aim, proposing a viable reuse of RG as a secondary raw material, in agreement with the European directive [54], waste valorization [55], and circular economy principles [56]. The reuse of RG waste in the ceramic industry has another important environmental implication, since it provides a low-cost secondary raw material (SRM) that substitutes a raw natural resource (i.e., clay minerals) contributing to the reduction of non-renewable resources exploitation.

6.2. The characteristics of SRM and corresponding ceramic products

The production of ceramics, both traditional and advanced, is one of the most investigated solutions for inorganic waste recycling (see Refs. [57,58] for a review), often offering high-quality products [59]. RG waste has a constant chemical composition, comparable over the years, thus providing a chemically and mineralogically reproducible secondary raw material, that is a fundamental requirement for possible industrial production. By comparing with previous RG chemical data from other industrial productions [6,11,49,60], the investigated samples reveal higher SO_3 and CaO and lower Fe_2O_3 and TiO_2 contents, suggesting that RG waste produced in Tuscany plant are purer than that of the Chinese, Malaysian, and Spanish plants.

Ceramic specimens experimentally produced in this study display comparable chemical and mineralogical compositions, but show slightly different microstructures. Indeed, CRG4 sample consists of coarser and more euhedral crystals than CRG1 sample, consistently to the higher processing temperature. As expected, the different temperature also affects porosity size and distribution. CRG1 has a total porosity of 22% compared to the 12% of samples CRG4; the equivalent diameter of pores is higher in CRG4 than in CRG1; the pore size distribution for CRG1 shows a higher frequency in the 10–40 μm size range designing a finer porosity than the CRG4 sample whereas the pore size distribution of CRG4 shows a greater proportion of larger pores (up to 90–100 μm), thus showing a less sorted porosity (Table 2S and Fig. 4S). The data shown here support the feasibility of a reproducible industrial production deriving from the fixedness of the starting SRM. In the ceramic products, the main crystalline phases are anhydride, Ca-pyroxene with minor Fe-oxides, and cassiterite (added in the ceramic mixture), finely intermixed

to an amorphous silicate matrix. Anhydride derives from gypsum dehydration below 200 °C (Table 2 and Fig. 1). It is worth noting that, based on DTA results, anhydrite transforms from a soluble to an insoluble phase, as testified by the occurrence of an exothermic signal in the range of 350–410 °C. The occurrence of insoluble anhydrite is a fundamental prerequisite for obtaining relatively low sulfate ion release in leaching tests (in progress). The anhydrous composition of starting gypsum and anhydrite is the same, except for Mg which is more abundant in RG than in the resulting anhydrite (Tables 1 and 3). The analyzed pyroxenes correspond to solid solutions between Ca- and Ca–Na pyroxenes, with variable Mg/Fe ratios, closer to augite and diopside in CRG1 and CRG4, respectively [38]. Most of the analyzed pyroxenes revealed variable Na and Al contents (Table 3), thus corresponding to the augite/aegirine-augite field. The crystallization of augite/aegirine pyroxenes clearly reflects the use of Na-silicatic fluxes in the ceramic mixture. EDS analyses do not allow the distinction between Fe^{2+} and Fe^{3+}, but it is possible to assume that the majority of Fe is in the form of 3+ oxidation state considering the sample storage conservation at open air and the oxidizing atmosphere during the heating process and consistently with the aegirine composition of pyroxene. Further, the observed chemical variability of pyroxenes is reasonably caused by locally variable equilibria during the heating process, as already observed for other Ca-rich silicate ceramics [34]. The amorphous matrix has a prevalent aluminosilicate composition with relatively low alkali content compared to standard glasses.

The main concern in the ceramic tests is represented by the occurrence of heavy elements, such as V and Cr, even if in low amounts, as revealed by XRF and EDS results. It is worth noting that based on SEM/EDS data, Cr is associated with Fe oxides, probably in the form of Cr^{3+} substituting Fe^{3+} in the oxide crystal structure [61], whereas V is preferentially partitioned in the glass matrix, probably in the 5+ oxidation state due to the ceramic kiln oxidizing atmosphere. This distribution may suggest an easier release of V from the amorphous matrix, compared to Cr, which is fixed within the crystal structure of the Fe oxide. However, the limited number of analyses carried out and the impossibility to determine with certainty the oxidation state of Cr and V only allow for speculative hypotheses. The mobility and solubility of these two elements depend on several physical and chemical factors, among which pH of the leaching agent, the mineralogical composition of raw materials and the firing temperatures at which ceramic bodies are fired [62]. Cr and V are often related to thermally unstable minerals that may breakdown during the ceramic firing process, leading to the formation of newly formed compounds. So, firing temperature could influence the mobilization and consequently the solubilization of these two elements to a great extent [62]. As detailed below, leaching tests on these ceramic products are in progress to determine the release elements from these ceramic products.

6.3. *Future investigations required for the lab-to-plant transition*

This paper represents the scientific background for further analyses that will be necessary to move from the lab experimental scale to an actual industrial plant. First, the ceramic material must be tested to determine its chemical and mechanical behavior. Leaching tests are in progress to determine the concentrations of the different chemical elements in the eluate, on the basis of the Italian law that defines the allowed limits for each element [63,64]. Moreover, we have performed preliminary tests on resistance, tensile strength and abrasion through Los Angeles and MicroDeval tests, according to EN-1097 and EN-1097-2 procedures to compare the mechanical properties of our products with those of traditional ceramics.

Another fundamental contribution to this work and future projects include careful economic analyses, such as cost/benefit analysis (CBA) to determine the economic advantages and disadvantages of the overall industrial process, pointing out possible criticisms and improving actions. Life cycle assessment (LCA) analysis will further support CBA, showing the details of the whole process, from the raw materials to the end products. LCA is a concrete and comprehensive tool to assess the environmental impacts of products from the cradle to the grave, the treatments, and the economies (the production of goodies) at a society level [65–67].

7. Conclusions

The management of huge volumes of RG wastes represent an impelling problem, with significant environmental, economic, and social implications. The investigated RG industrial waste denotes constancy over the time. The data, covering approximately 10 years production, are also in complete agreement with previous data reported in bibliography as well as by periodic surveys done by the Regional Agency of Environmental protection of Tuscany (ARPAT). Other features of this research are represented by: 1) the large availability and the reproducibility of RG waste, that may be used as a low-cost secondary raw material; 2) the extraordinarily high % of RG waste used as SRM, replacing natural not renewable resources; 3) the relatively low T required to convert RG waste into a new ceramic product (never exceeding 1000 °C). This supports the hypothesis of the economic and environmental sustainability of the process, which could be further refined through other future tests with slightly different mixtures of RG waste and additives in order to realize the most suitable eutectic mixtures at even lower temperatures.

Author contributions

All authors contributed to the study conception and design. Conceptualization, Visualization, Data curation, Elaboration of experimental data, Paper writing, reviewing & editing: Narcisa Mihaela Marian. Conceptualization, Elaboration of experimental data, Paper writing, reviewing & editing: Matteo Perotti. SEM/EDS Investigation, Draft review & editing: Carlo Indelicato. Thermal analyses investigation, Draft review & editing: Claudia Magrini. SEM/EDS Investigation, Draft review & editing: Giovanna Giorgetti. XRF investigation, Draft review & editing: Giancarlo Capitani. Supervision, Project administration, Funding acquisition, Conceptualization, Visualization, Paper writing, review & editing: Cecilia Viti.

Declaration of competing interest

The authors declare that they have no known competing financial interests or personal relationships that could have appeared to influence the work reported in this paper.

Acknowledgments

GRINN srl is kindly acknowledged for providing the ceramic tests. We thank Elin Jannings for her precious contribution to the language review.

This research did not receive any specific grant from funding agencies in the public, commercial, or not-for-profit sectors.

Appendix A. Supplementary data

Supplementary data to this article can be found online at https://doi.org/10.1016/j.ceramint.2023.01.086.

References

[1] J. Rees, Natural Resources: Allocation, Economics and Policy, Routledge, 2017.
[2] E. Commission, I. Directorate-General for Internal Market Entrepreneurship and SMEs, S. Bobba, P. Claudiu, D. Huygens, P. Alves Dias, B. Gawlik, E. Tzimas, D. Wittmer, P. Nuss, M. Grohol, H. Saveyn, F. Buraoui, G. Orveillon, T. Hámor, S. Slavko, F. Mathieux, M. Gislev, C. Torres De Matos, G. Blengini, F. Ardente,

D. Blagoeva, E. Garbarino, Report on Critical Raw Materials and the Circular Economy, Publications Office, 2018, https://doi.org/10.2873/167813.
[3] OECD, Material Resources, Productivity and the Environment, OECD, 2015. https://www.oecd-ilibrary.org/environment/material-resources-productivity-and-the-environment_9789264190504-en.
[4] A. Jiménez-Rivero, J. García-Navarro, Management of end-of-life gypsum in a circular economy, in: Advances in Construction and Demolition Waste Recycling, Elsevier, 2020, pp. 69–79, https://doi.org/10.1016/b978-0-12-819055-5.00005-x.
[5] J. Ju, Y. Feng, H. Li, B. Wang, A novel approach for separation and recovery of titanium, scandium, iron from acidic wastewater and red gypsum utilization, Min. Metall. Explor. 39 (2022) 1297–1312, https://doi.org/10.1007/s42461-022-00600-5.
[6] M.Y. Mohd Tadza, N. Mazelan, N.F. Yusri, A. Abdullah, Some geotechnical properties of pure and waste gypsum for geoelectrical grounding applications, Civ. Environ. Eng. Rep. 29 (2019) 97–106, https://doi.org/10.2478/ceer-2019-0027.
[7] M.J. Gázquez, J.P. Bolívar, R. Garcia-Tenorio, F. Vaca, A review of the production cycle of titanium dioxide pigment, Mater. Sci. Appl. (2014) 441–458, https://doi.org/10.4236/msa.2014.57048, 05.
[8] T. Ginsberg, M. Modigell, W. Wilsmann, Thermochemical characterisation of the calcination process step in the sulphate method for production of titanium dioxide, Chem. Eng. Res. Des. 89 (2011) 990–994, https://doi.org/10.1016/J.cherd.2010.11.006.
[9] G.S. McNulty, Production of titanium dioxide, in: Proceedings of NORM V International Conference, Citeseer, Seville, Spain, 2007, pp. 169–189.
[10] M.J. Gázquez, M. Contreras, S.M. Pérez-Moreno, J.L. Guerrero, M. Casas-Ruiz, J. P. Bolívar, A review of the commercial uses of sulphate minerals from the titanium dioxide pigment industry: the case of Huelva (Spain), Minerals 11 (2021), https://doi.org/10.3390/min11060575.
[11] M.J. Gázquez, J.P. Bolívar, R. García-Tenorio, F. Vaca, Physicochemical characterization of raw materials and co-products from the titanium dioxide industry, J. Hazard Mater. 166 (2009) 1429–1440, https://doi.org/10.1016/j.jhazmat.2008.12.067.
[12] A. Colak, The long-term durability performance of gypsum–Portland cement–natural pozzolan blends, Cement Concr. Res. 32 (2002) 109–115, https://doi.org/10.1016/S0008-8846(01)00637-8.
[13] G. Frigione, Gypsum in cement, in: Advances in Cement Technology, Elsevier, 1983, pp. 485–535, https://doi.org/10.1016/b978-0-08-028670-9.50020-x.
[14] G. Protano, D. Baroni, S. Bianchi, C. Russo, M. Salleolini, Assessing the impact on groundwater chemistry of an environmental restoration performed using industrial solid waste from TiO2 production, Appl. Geochem. 120 (2020), 104666, https://doi.org/10.1016/j.apgeochem.2020.104666.
[15] N.A. Rosli, H.A. Aziz, M.R. Selamat, L.L.P. Lim, A mixture of sewage sludge and red gypsum as an alternative material for temporary landfill cover, J. Environ. Manag. 263 (2020), 110420, https://doi.org/10.1016/j.jenvman.2020.110420.
[16] N.A. Rosli, H.A. Aziz, M.R. Selamat, L.L.P. Lim, M.H. Zawawi, Effect of compaction on physical properties of a sewage sludge and red gypsum mixture as intermediate landfill cover, Construct. Build. Mater. 289 (2021), 123153, https://doi.org/10.1016/j.conbuildmat.2021.123153.
[17] R.A. Kamarudin, M.S. Zakaria, The utilization of red gypsum waste for glazes, Malays. J. Anal. Sci. 11 (2007) 57–64.
[18] M.J. Gazquez, J.P. Bolivar, F. Vaca, R. García-Tenorio, A. Caparros, Evaluation of the use of TiO2 industry red gypsum waste in cement production, Cem. Concr. Compos. 37 (2013) 76–81, https://doi.org/10.1016/j.cemconcomp.2012.12.003.
[19] Y. Zhang, F. Wang, H. Huang, Y. Guo, B. Li, Y. Liu, P.K. Chu, Gypsum blocks produced from TiO2 production by-products, Environ. Technol. 37 (2016) 1094–1100, https://doi.org/10.1080/09593330.2015.1102329.
[20] J. Zhang, Y. Yan, Z. Hu, Preparation and characterization of foamed concrete with Ti-extracted residues and red gypsum, Construct. Build. Mater. 171 (2018) 109–119, https://doi.org/10.1016/j.conbuildmat.2018.03.072.
[21] Q. Cai, B. Ma, J. Jiang, J. Wang, Z. Shao, Y. Hu, B. Qian, L. Wang, Utilization of waste red gypsum in autoclaved aerated concrete preparation, Construct. Build. Mater. 291 (2021), 123376, https://doi.org/10.1016/J.CONBUILDMAT.2021.123376.
[22] C.I. Fauziah, M.N. Hanani, S. Zauyah, A.W. Samsuri, A. Rosazlin, Co-Application of red gypsum and sewage sludge on acidic tropical soils, Commun. Soil Sci. Plant Anal. 42 (2011) 2561–2571, https://doi.org/10.1080/00103624.2011.614032.
[23] J. Schindelin, I. Arganda-Carreras, E. Frise, V. Kaynig, M. Longair, T. Pietzsch, S. Preibisch, C. Rueden, S. Saalfeld, B. Schmid, J.-Y. Tinevez, D.J. White, V. Hartenstein, K. Eliceiri, P. Tomancak, A. Cardona, Fiji: an open-source platform for biological-image analysis, Nat. Methods 9 (2012) 676–682, https://doi.org/10.1038/nmeth.2019.
[24] W. Smykatz-Kloss, Differential Thermal Analysis: Application and Results in Mineralogy, Springer Science & Business Media, 2012.
[25] A.E. Charola, J. Pühringer, M. Steiger, Gypsum: a review of its role in the deterioration of building materials, Environ. Geol. 52 (2007) 207–220, https://doi.org/10.1007/s00254-006-0566-9.
[26] D. Freyer, W. Voigt, Crystallization and phase stability of $CaSO_4$ and $CaSO_4 \cdot$ based salts, Monatsh. Chem. 134 (2003) 693–719, https://doi.org/10.1007/s00706-003-0590-3.
[27] D.L. Hudson-Lamb, C.A. Strydom, J.H. Potgieter, The thermal dehydration of natural gypsum and pure calcium sulphate dihydrate (gypsum), Thermochim. Acta 282–283 (1996) 483–492, https://doi.org/10.1016/0040-6031(95)02819-6.
[28] V.S. Ramachandran, R.M. Paroli, Handbook of Thermal Analysis of, Andrew Publishing, 2002.
[29] R.R. West, W.J. Sutton, Thermography of gypsum, J. Am. Ceram. Soc. 37 (1954) 221–224, https://doi.org/10.1111/j.1151-2916.1954.tb14027.x.
[30] P. Ballirano, E. Melis, Thermal behavior of β-anhydrite CaSO4 to 1,263 K, Phys. Chem. Miner. 34 (2007) 699–704, https://doi.org/10.1007/s00269-007-0186-2.
[31] H. Javangula, Q. Lineberry, Comparative studies on fire-rated and standard gypsum wallboard, in: J Therm Anal Calorim, Kluwer Academic Publishers, 2014, pp. 1417–1433, https://doi.org/10.1007/s10973-014-3795-2.
[32] S. Follner, A. Wolter, K. Helming, C. Silber, H. Bartels, H. Follner, On the real structure of gypsum crystals, Cryst. Res. Technol. 37 (2002) 207–218, https://doi.org/10.1002/1521-4079(200202)37:2/3<207::AID-CRAT207>3.0.CO;2-L.
[33] P. Bayless, Mineral Powder Diffraction File, Data Book, International Centre for Diffraction Data. JCPDS, Swarthmore, PA 19081, USA, 1986.
[34] M. Dondi, G. Ercolani, B. Fabbri, M. Marsigli, An approach to the chemistry of pyroxenes formed during the firing of Ca-rich silicate ceramics, Clay Miner. 33 (1998) 443–452, https://doi.org/10.1180/000985598545741.
[35] M. Dondi, M. Raimondo, C. Zanelli, Clays and bodies for ceramic tiles: reappraisal and technological classification, Appl. Clay Sci. 96 (2014) 91–109, https://doi.org/10.1016/j.clay.2014.01.013.
[36] G.A. Khater, Y. Yue, M.O. Abu Safiah, M.A. Mahmoud, Synthesis and characterization of anorthite and magnetite glass-ceramics from basaltic rocks, Silicon 11 (2019) 1763–1774, https://doi.org/10.1007/s12633-018-9991-0.
[37] E. Gliozzo, Ceramic technology. How to reconstruct the firing process, Archaeol. Anthropol. Sci. 12 (2020) 260, https://doi.org/10.1007/s12520-020-01133-y/Published.
[38] N. Morimoto, Nomenclature of pyroxenes, Mineral. Petrol. 39 (1988) 55–76, https://doi.org/10.1007/BF01226262.
[39] M. Shakeel, F. Jabeen, S. Shabbir, M.S. Asghar, M.S. Khan, A.S. Chaudhry, Toxicity of nano-titanium dioxide (TiO2-NP) through various routes of exposure: a review, Biol. Trace Elem. Res. 172 (2016), https://doi.org/10.1007/s12011-015-0550-x.
[40] A. Weir, P. Westerhoff, L. Fabricius, K. Hristovski, N. von Goetz, Titanium dioxide nanoparticles in food and personal care products, Environ. Sci. Technol. 46 (2012) 2242–2250, https://doi.org/10.1021/es204168d.
[41] X. Tian, X. Cui, T. Lai, J. Ren, Z. Yang, M. Xiao, B. Wang, X. Xiao, Y. Wang, Gas sensors based on TiO2 nanostructured materials for the detection of hazardous gasses: a review, Nano Mater. Sci. 3 (2021) 390–403, https://doi.org/10.1016/J.NANOMS.2021.05.011.
[42] S. Jafari, B. Mahyad, H. Hashemzadeh, S. Janfaza, T. Gholikhani, L. Tayebi, Biomedical Applications of TiO 2 Nanostructures: Recent Advances, 2020, https://doi.org/10.2147/IJN.S249441.
[43] A.J. Haider, Z.N. Jameel, I.H.M. Al-Hussaini, Review on: titanium dioxide applications, Energy Proc. 157 (2019) 17–29, https://doi.org/10.1016/j.egypro.2018.11.159.
[44] B. Liang, C. Li, C. Zhang, Y. Zhang, Leaching kinetics of Panzhihua ilmenite in sulfuric acid, Hydrometallurgy 76 (2005) 173–179, https://doi.org/10.1016/j.hydromet.2004.10.006.
[45] X. Wang, C. Li, H. Yue, S. Yuan, C. Liu, S. Tang, B. Liang, Effects of mechanical activation on the digestion of ilmenite in dilute H2SO4, Chin. J. Chem. Eng. 27 (2019) 575–586, https://doi.org/10.1016/J.CJCHE.2018.06.020.
[46] M. Amirul Hakim Sidek, R.M. Yunus, M. Al-Nizar Khan Ahmad Khan, M. Remanul Islam, Industrial Operation Feasibility for Red Gypsum-Based Brick Manufacturing, 2019. www.ajouronline.com.
[47] I. Fauziah, S. Zauyah, T. Jamal, Characterization and land application of red gypsum: a waste product from the titanium dioxide industry, Sci. Total Environ. 188 (1996) 243–251, https://doi.org/10.1016/0048-9697(96)05179-0.
[48] M.J. Gazquez, J.P. Bolivar, F. Vaca, R. García-Tenorio, A. Caparros, Evaluation of the use of TiO2 industry red gypsum waste in cement production, Cem. Concr. Compos. 37 (2013) 76–81, https://doi.org/10.1016/j.cemconcomp.2012.12.003.
[49] Q. Chen, W. Ding, H. Sun, T. Peng, Synthesis of anhydrite from red gypsum and acidic wastewater treatment, J. Clean. Prod. 278 (2021), 124026, https://doi.org/10.1016/J.JCLEPRO.2020.124026.
[50] I. v Muralikrishna, V. Manickam, in: I. v Muralikrishna, V.B.T.-E.M. Manickam (Eds.), Chapter Thirteen - Industrial Wastewater Treatment Technologies, Recycling, and Reuse, Butterworth-Heinemann, 2017, pp. 295–336, https://doi.org/10.1016/B978-0-12-811989-1.00013-0.
[51] T.H. Kim, S.H. Tae, C.U. Chae, W.Y. Choi, The environmental impact and cost analysis of concrete mixing blast furnace slag containing titanium gypsum and sludge in South Korea, Sustainability (2016) 8, https://doi.org/10.3390/su8060502.
[52] ARPAT, Accordo volontario sul riutilizzo dei gessi rossi Tioxide per il ripristino ambientale della ex cava di Poggio Speranzona, 2010. Grosseto.
[53] ARPAT, Recupero ambientale e morfologico della ex cava di quarzite di Poggio Speranzona di Montioni (comune di Follonica) con gessi rossi della Venatori Italy Srl di Scarlino, 2018.
[54] European Parliament and of the Council, Directive 2008/98, EC of the European Parliament and of the Council, 2008, https://doi.org/10.5040/9781782258674.0028.
[55] N. Leder, M. Kumar, V.S. Rodrigues, Influential factors for value creation within the circular economy: framework for waste valorisation, Resour. Conserv. Recycl. 158 (2020), 104804, https://doi.org/10.1016/j.resconrec.2020.104804.
[56] F.F. Martins, H. Castro, Raw material depletion and scenario assessment in European Union – a circular economy approach, Energy Rep. 6 (2020) 417–422, https://doi.org/10.1016/j.egyr.2019.08.082.
[57] S.S. Hossain, P.K. Roy, Sustainable ceramics derived from solid wastes: a review, J. Asian Ceram. Soc. 8 (2020) 984–1009, https://doi.org/10.1080/21870764.2020.1815348.
[58] C. Zanelli, S. Conte, C. Molinari, R. Soldati, M. Dondi, Waste recycling in ceramic tiles: a technological outlook, Resour. Conserv. Recycl. 168 (2021), 105289, https://doi.org/10.1016/J.RESCONREC.2020.105289.

[59] K. Sung, A review on upcycling: current body of literature, knowledge gaps and a way forward, Int. Conf. Environ. Cult. Econ. Soc. Sustain. 17 (2015) 28–40. http://irep.ntu.ac.uk/id/eprint/12706/1/219287_PubSub1825_Sung.pdf.

[60] M. C.-R, J.P. B, Manuel Jesús Gázquez, Manuel Contreras, Silvia María Pérez-Moreno, Jose Luis Guerrero, A Review of the Commercial Uses of Sulphate Minerals from the Titanium Dioxide Pigment Industry : the Case of Minerals, 2021.

[61] I.T. Burke, W.M. Mayes, C.L. Peacock, A.P. Brown, A.P. Jarvis, K. Gruiz, Speciation of arsenic, chromium, and vanadium in red mud samples from the Ajka spill site, Hungary, Environ. Sci. Technol. 46 (2012) 3085–3092, https://doi.org/10.1021/es3003475.

[62] M. Dondi, B. Fabbri, C. Mingazzini, Mobilisation of chromium and vanadium during firing of structural clay products, ZI International 50 (1997) 685–696.

[63] Italian Decree Minister, Individuazione dei rifiuti non pericolosi sottoposti alle procedure semplificate di recupero ai sensi degli articoli 31 e 33 del decreto legislativo n. 22, GU Serie Generale n, 1998, 88 del 16-04-1998 - Suppl. Ordinario n. 72.

[64] Italian Decree Minister, 152. Norme in Materia Ambientale. GU Serie Generale N. 88, 2006 del 14 aprile 2006 - Supplemento Ordinario n. 96.

[65] Z. Chen, L. Huang, Application review of LCA (life cycle assessment) in circular economy: from the perspective of PSS (product service system), Proc. CIRP 83 (2019) 210–217, https://doi.org/10.1016/J.PROCIR.2019.04.141.

[66] M. Haupt, M. Zschokke, How can LCA support the circular economy?—63rd discussion forum on life cycle assessment, Zurich, Switzerland, November 30, 2016, Int. J. Life Cycle Assess. 22 (2017) 832–837, https://doi.org/10.1007/s11367-017-1267-1.

[67] K. Tóth Szita, The application of life cycle assessment in circular economy, Hungar. Agric. Eng. (2017) 5–9, https://doi.org/10.17676/hae.2017.31.5.